Study on shock wave-induced cavitation bubbles dissolution process*

Huan Xu(许欢)[1,2,†], Peng-Fei Fan(范鹏飞)[1,†], Yong Ma(马勇)[3], Xia-Sheng Guo(郭霞生)[1], Ping Yang(杨平)[2], Juan Tu(屠娟)[1,‡], and Dong Zhang(章东)[1,§]

[1] *Key Laboratory of Modern Acoustics of the Ministry of Education, Nanjing University, Nanjing* 210093, *China*
[2] *National Institute of Metrology, Beijing* 100029, *China*
[3] *Institute of Traumatology and Orthopedics, Nanjing University of Chinese Medicine, Nanjing* 210023, *China*

(Received 10 October 2016; revised manuscript received 14 November 2016; published online 20 December 2016)

This study investigated dissolution processes of cavitation bubbles generated during *in vivo* shock wave (SW)-induced treatments. Both active cavitation detection (ACD) and the B-mode imaging technique were applied to measure the dissolution procedure of biSpheres contrast agent bubbles by *in vitro* experiments. Besides, the simulation of SW-induced cavitation bubbles dissolution behaviors detected by the B-mode imaging system during *in vivo* SW treatments, including extracorporeal shock wave lithotripsy (ESWL) and extracorporeal shock wave therapy (ESWT), were carried out based on calculating the integrated scattering cross-section of dissolving gas bubbles with employing gas bubble dissolution equations and Gaussian bubble size distribution. The results showed that (i) B-mode imaging technology is an effective tool to monitor the temporal evolution of cavitation bubbles dissolution procedures after the SW pulses ceased, which is important for evaluation and controlling the cavitation activity generated during subsequent SW treatments within a treatment period; (ii) the characteristics of the bubbles, such as the bubble size distribution and gas diffusion, can be estimated by simulating the experimental data properly.

Keywords: bubble cavitation, shock wave, B-mode imaging, residual bubbles, bubble dissolution

PACS: 43.25.Yw, 43.35.Wa, 43.80.+p **DOI:** 10.1088/1674-1056/26/2/024301

1. Introduction

High intensity focused ultrasound (HIFU) is widely applied as a non-invasive technique in clinical diagnose and therapy, including hemostasis, thrombolysis, shock wave (SW) treatments, ultrasonic drug delivery, and lately in treatment for painful conditions.[1–5] Taking advantage of the non-invasive, small, well-circumscribed thermal lesion, extracorporeal shock wave lithotripsy (ESWL) has been widely applied for stone disease treatments in the past few decades.[3,6–8] Despite these impressive therapeutic effects, there is non-ignorable evidence that ESWL causes tissue injury, such as hematomas, hematuria, renal and perirenal hemorrhage, and kidney enlargement.[9,10] Including the above tissue damage caused by cavitation, bubbles formed in the propagation path scatter and absorb much of the acoustical energy before it reaches the target area. Furthermore, it also changes the focal zone location in the target tissue.[11] Many efforts have been made to control the cavitation in SW-induced treatments.[6,12–15] It is reported that the bubble cavitation could be suppressed by a small overpressure or slow pulse repetition frequency during ESWL.[12,13] Evan *et al.* pointed out that kidney damage and renal functional changes could be minimized by waveform control that reduces cavitation in shock wave lithotripsy (SWL).[6] Zhong and Zhou developed an in-situ pulse superposition technique to suppress large intraluminal bubble expansion without weakening the curative effect.[14,15]

Although primary cavitation excited by SWs is crucial to the stone comminution, the residual daughter bubbles accompanying the collapse of cavitation bubbles also play an important role.[7,16–19] These residual daughter bubbles can persist from one shock to the next, in the order of one second.[18] On one hand, these bubbles will attenuate the amplitude of the next SW and delay the time for the SW to reach the stone,[13,19] which leads to weakening stone comminution efficiency. The influence is more significant at higher pulse-repetition frequency (PRF), as less time is available for residual daughter bubbles to passively dissolve between sequent SWs. In order to enhance the comminution efficiency, Duryea *et al.* developed an active residual bubble removal method.[20,21] They suggested that adjusting the cavitation environment can improve comminution efficiency when PRF is at a high rate. On the other hand, residual bubbles may also act as nuclei that can be excited by subsequent pulses. Therefore, the residual bubbles may improve the therapeutic effect,[7] or cause further tissue damage. Therefore, it may be favorable

*Project partially supported by the National Natural Science Foundation of China (Grant Nos. 81627802, 81473692, 81673995, 11374155, 11574156, 11474001, 11474161, 11474166, and 11674173), Natural Science Foundation of Jiangsu Province, China (Grant No. BK20151007), and the Qing Lan Project of Jiangsu Province, China.

†These authors contributed equally to this work.
‡Corresponding author. E-mail: juantu@nju.edu.cn
§Corresponding author. E-mail: dzhang@nju.edu.cn

© 2017 Chinese Physical Society and IOP Publishing Ltd

to achieve an optimal SW treatment[7,13,22] by adjusting the dissolving process of residual cavitation bubbles between two sequent SWs.

It is known that free gas bubbles present in a liquid are usually unstable, which means they will tend to dissolve due to the external pressure generated by surface tension that will force the gas out of the bubble into solution in the liquid. Epstein and Plesset developed equations that can be used to calculate the expected lifetime of an air bubble in an unbounded liquid.[23] Effects have been done to observe the UCA dissolution process by the ACD system during *in vitro* experiments.[24] However, the dissolution process of gas bubbles generated *in vivo* is not yet well known. Therefore, we intended to investigate the dissolution processes of cavitation bubbles generated during *in vivo* SW treatments. The general hypotheses tested in this study were: (i) B-mode imaging is an effective technique to monitor the dissolution procedure of cavitation bubbles; and (ii) the cavitation bubble dissolution procedure detected by B-mode ultrasound can be simulated based on the calculation of scattering cross-section with employing gas bubble dissolution equations and Gaussian bubble size distribution. Firstly, *in vitro* experiments were conducted to monitor the dissolution process of biSpheres contrast agent bubbles using both the single-transducer ACD system and B-mode ultrasound imaging system. To verify the efficiency of the B-mode imaging system, its collected signals were compared with the signals detected by the ACD system, which had been proved to be capable of detecting microbubbles destruction and the subsequent dissolution process.[24] Furthermore, the normalized decay curves of hyperechoic regions measured by the B-mode imaging system[25] during both *in vivo* ESWL treatments of pig kidneys and *in vivo* ESWT treatments of plantar fasciitis. The results showed that monitoring bubble dissolution procedures using B-mode imaging could provide a better understanding of the temporal evolution of cavitation bubbles after SW pulses ceased *in vivo*. In addition, the characteristics of cavitation bubbles, such as the bubble size distribution and gas diffusion, can be estimated by simulating the experimental data properly.

2. Theory

The purpose of this paper was to simulate the cavitation bubble dissolution process detected after SW treatments in ESWL and ESWT. Because the experimental data were collected using B-mode ultrasound, the simulation should be based on the calculation of the backscattering cross-section. Furthermore, the simulation should also include the effects of bubble size distribution, because the detected signals involved the scattering from a distribution of bubbles. Therefore, the final simulation should incorporate the changing radius of the dissolving bubbles, $R(t)$, into the scattering cross-section equations, taking into account the bubble size distribution. Chen *et al.*[24] performed just this type of analysis using standard ACD in an *in vitro* setting by monitoring the destruction of ultrasound contrast agents (UCA) microbubbles. The results were quite good, and thus we will use their simulation and analysis techniques for our purposes.

2.1. Bubble dissolution

It is known in an *in vivo* setting, bubble dissolution is complicated because they can be stabilized by other surfaces or coatings, or they might move because of blood flow, or there might be bubble-bubble interactions. We will simplify the process by assuming that the dissolution is from an unbounded liquid, without interactions. We hypothesize that discrepancies between the simulations and data are most probably due to the effects mentioned. The dissolution rate of a gas bubble in liquid can be calculated by the following equation:[23]

$$\frac{\mathrm{d}R}{\mathrm{d}t} = -D_{\mathrm{A}}L_{\mathrm{A}}\frac{1-\dfrac{c_\infty}{c_0}+\dfrac{\tau}{R\rho_{\mathrm{g}}}}{1+\dfrac{2\tau}{3R\rho_{\mathrm{g}}}}\left(\frac{1}{R}+\frac{1}{\sqrt{\pi D_{\mathrm{A}}t}}\right), \tag{1}$$

where $\tau = 2M\sigma/R_{\mathrm{G}}T$, t is time, C_∞ is the concentration of dissolved gas in solution, C_0 is the saturation concentration of dissolved gas, and M is the molecular weight of gas.

Other parameters are defined in Table 1. The initial bubble radius condition used in the calculation was R_0, which corresponded to the equilibrium bubble radius at t=0.

2.2. Calculation of bubble scattering cross-section

Once we know the size of a bubble at any time, we can then calculate its scattering cross section as a function of time based on the assumption of the scattering from small particles with the wavelength $\lambda \gg R$:[27]

$$\sigma_{\mathrm{s}} = 4\pi a_{\mathrm{e}}^2\frac{\Omega^4}{(\Omega^2-1)^2+\Omega^2\delta^2}, \tag{2}$$

$$\Omega = \omega/\omega_0, \tag{3}$$

$$\delta = \delta_{\mathrm{th}}+\delta_\eta+\delta_{\mathrm{R}}. \tag{4}$$

Thermal damping constant:

$$\delta_{\mathrm{th}} = \frac{3p_0}{\omega_0\omega\rho_l a_{\mathrm{e}}^2}\,\mathrm{Im}\left(\frac{1}{\Phi}\right), \tag{5a}$$

$$\Phi(a_{\mathrm{e}},\omega) = \frac{1}{\gamma}\left[1+\frac{3(\gamma-1)}{X^2}(X\coth X-1)\right], \tag{5b}$$

$$X(a_{\mathrm{e}},\omega) = a_{\mathrm{e}}\sqrt{\frac{\mathrm{i}\omega\rho_{\mathrm{g}}C_p}{K_{\mathrm{g}}}}. \tag{5c}$$

Radiation resistance damping constant

$$\delta_{\mathrm{R}} = \frac{\omega^2 a_{\mathrm{e}}}{\omega_0 c}. \tag{6}$$

Viscosity damping constant

$$\delta_\eta = \frac{4\eta_{\mathrm{L}}}{\omega_0\rho_{\mathrm{L}}a_{\mathrm{e}}^2}, \tag{7}$$

where a_e is the equilibrium bubble radius, ω is the frequency, ω_0 is the resonance frequency, and p_0 is the hydrostatic pressure. Other parameters are listed in Table 1.

With a scaling factor, the square root of the scattering cross section can be used to simulate the expected scattering amplitude *vs.* time that we would see on a B-mode image.

2.3. Size distribution of bubbles

During ESWL or ESWT treatment, bubble 'clusters' are generated by shock wave pulses, rather than single bubbles. The size distribution of these bubbles is not homogeneous. For simplicity, a Gaussian function[24] with mean radius of R_0 and standard deviation of SD will be employed to cavitation bubble size distribution $W(R_0)$:

$$W(R_0) = \frac{1}{\sqrt{2\pi}(SD)} \exp\left[-\frac{(RR-R_0)^2}{2(SD)^2}\right], \tag{8}$$

where RR is in range of radii.

The bubble size distribution was considered as a weighting factor when the scattering cross section was calculated. Thus, the final simulated scattering cross-section for a distribution of bubbles is given by:

$$\sigma_s(R_0) = W(R_0)\sigma_s. \tag{9}$$

2.4. Best fitting standard

We hypothesized that the measured bubble dissolution curves could be simulated by calculating the backscattering cross-sections, while employing the bubble dissolution equation and assuming a Gaussian size distribution. Three unknown parameters were chosen for the simulation: R_0, SD, and D_A, while assuming other parameters to be constant (See Table 1). Minimum standard deviation of error (SDE) evaluation was applied to determine the best fitting result.

Table 1. Notations used for bubble dissolution calculation.

Variable	Parameter	Simulation value
D_A	diffusion constant of air	2×10^{-9} m^2/s
L_A	Ostwald coefficient of air	1.71×10^{-2}
R_G	gas constant	8.314 J/mole·K
T	temperature	300 K
σ	surface tension	0.07275 N/m
ρ_g	gas density	1.161 kg/m^3
η_L	liquid shear viscosity, from Church *et al.*, 1995[26]	0.001 Pa·s
ρ_L	density of a Newtonian liquid	10^3 kg/m
C_p	heat capacity at constant pressure, from CRC handbook	240.67
K_g	thermal conductivity, from CRC handbook, for air at 300 K and 1 atm	0.00626
c	acoustic velocity in the liquid	1500 m/s
γ	gas adiabatic constant	1.07

3. *In vitro* UCA bubble dissolution detected by ACD and B-mode systems

3.1. Material and methods

3.1.1. Ultrasound contrast agents

For the *in vitro* experiments, we used ultrasound contrast agents as the starting point because they have a well-defined size distribution. That is, we know *a priori* pretty much what the initial bubble size distribution will be. The ultrasound contrast agent used in this study was biSpheres (Point Biomedical, San Carlos, CA). BiSpheres is an experimental contrast agent with air enclosed by an inner polymer and an outer albumin shell. The biSpheres preparations were provided in powder form, and were reconstituted with distilled water before use according to the manufacturer's recommended protocol. According to the manufacturer's data, the mean diameter of biSpheres is 40 μm, and there are approximately 5×10^8 microbubbles/ml for biSpheres.

3.1.2. Experimental setup

Figure 1 shows the diagram of the experimental setup used in this study. The *in vitro* experiments were performed in a $16.5\times12.5\times12.5$ cm^3 acrylic tank filled with deionized, filtered water, which was left overnight to achieve an equilibrium gas saturation concentration. A 5-MHz single-element ACD transducer was mounted onto one side of the tank, and a B-mode probe (L38, Sonosite 180, Bothell, WA) was attached to the quadrature sidewall with ultrasonic gel applied to provide good acoustic coupling. The scanning plane of the B-mode imager overlapped with the focal region of the ACD transducer. A pipette bulb was used to contain the sample UCA suspension and placed in the co-focal region of the B-mode probe and the 5-MHz transducer. The scanner imaged from the top of the pipette bulb.

The 5-MHz transducer was driven by a pulse-receiver (5072, Panametrics, Waltham, MA, USA) whose output signal was triggered by the function generator (33120A, Hewlett Packard, Loveland, CO). The ACD interrogating pulses

(10 cycles, 5 MHz, PRF = 5 kHz) with low amplitude were sent to detect the bubble dissolution. Relative high PRF (5 kHz) and low amplitude (about 20 kPa) which was definitely lower than the cavitation threshold were applied to ensure that the bubbles remained relatively stationary over short time scales. Then the echoes scattering by bubbles were recorded continuously using the sequence mode of the oscilloscope (LC 334 AM, Lecroy, Chestnut Ridge, NY). The detected waveforms were digitized by the oscilloscope at a resolution of 40 ns/pt. The hold-off interval of the interrogating pulses was adjusted to ensure the data collecting time was long enough to observe the entire bubble dissolution process. The whole process for recording one ACD waveform lasted about 0.029 s, including sending interrogating pulses, receiving scattering signals, and recording and saving them into the computer. A total of 1452 20-μs-long ACD waveforms were detected and stored for every sample.

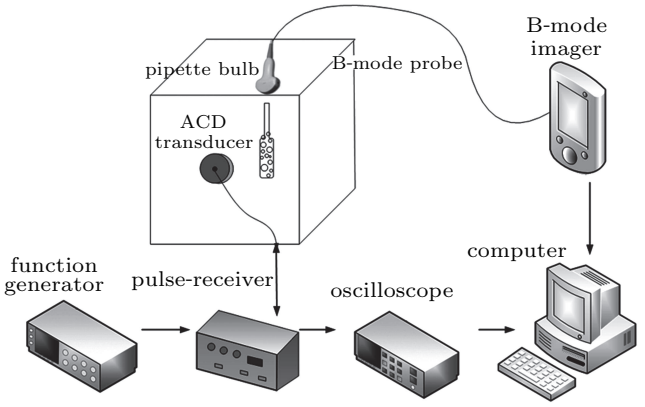


Fig. 1. Diagram of the experimental setup.

The bubble dissolution processes were also imaged using the B-mode system at a frame rate of 30 frames/s. The B-mode movies were digitized through a digital video converter (Px-AV100U, Plextor Inc., Fremont, CA), before being transferred to the computer. All the recorded ACD signals and B-mode movies were stored in PC computers, subsequently processed offline by the MatLab program (Math Works, Natick, MA).

3.1.3. Image processing method

The areas of the hyperechoic regions in the B-mode images were quantified after image processing had been done by MatLab programs (Mathworks, Natick, MA). The image processing method is the same as the one described in our previous work.[16] Briefly, the area of the hyperechoic region was detected and quantified in terms of pixels by an image binarization method. Then, the images were processed frame by frame to observe the temporal evolution of the hyperechoic regions.

3.2. Experimental results

This *in vitro* study was designed to verify the feasibility of monitoring the bubble dissolution process with B-mode ultrasound, by comparing the signals detected using B-model ultrasound with that obtained from ACD system.

Before the experiments, 1 ml of biSpheres bubbles was withdrawn and diluted immediately in 1000 ml of distilled water. For every study, only 1 ml of diluted suspension was injected to the pipette bulb using a syringe with an 18-gauge needle. Because the original concentration of biSpheres is about 5×10^8 microbubbles/ml, $\sim 5\times10^5$ microbubbles were therefore presented in the pipette bulb.

Interrogating pulses were sent by the 5-MHz ACD transducer to detect the presence of UCA microbubbles. The amount of bubbles was quantified according to the amplitude of the backscattered interrogating signal. Meanwhile, the bubble dissolution process was also monitored using B-mode ultrasound. The time-varying bubble numbers were assumed to be proportional to the area quantification of the hyperechoic spots recorded in the B-mode movies. Both the ACD and B-mode data collection were stopped simultaneously, when almost all the bright bubble echoes disappeared in the B-mode image. Five replicate experiments were performed and the data were averaged. In order to compare the results obtained with these two systems, all the signals were normalized to the corresponding maximum value. Then, the experimental data were simulated according to the scattering cross-section calculation with 3 fitting parameters (e.g., mean radius of bubbles R_0, standard deviation of bubble size distribution SD and gas diffusion constant D_A). The best fitting standard was applied to achieve the minimum standard deviation of error.

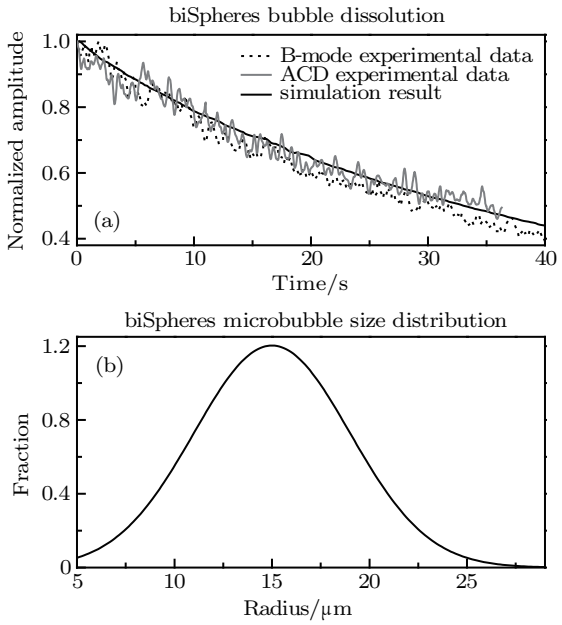


Fig. 2. Comparison between the ACD and B-mode experimental data, and the simulation results for the experimental data. (a) Comparison between the experimental data and the simulation results. The experimental data could be best fitted with the following parameter sets: the mean diameter of bubbles $R_0 = 15$ μm, the standard deviation of bubbles distribution $SD = 4$ μm, and the diffusion constant $D_A = 2.5\times10^{-9}$ m^2/s. (b) The bubble size distribution.

The results were shown in Fig. 2. The normalized experimental data obtained from the B-mode and ACD systems show good consistency, which prove that the B-mode system is an effective tool to quantify the bubble behaviors. It is also shown in the figure that the dissolution curves, which were obtained with both ACD and B-mode systems, agree very well with simulation results. The best fitting parameters for the simulation result were selected as: mean diameter of bubbles $R_0 = 15$ μm, the standard deviation of bubbles distribution $SD = 4$ μm, and the diffusion constant $D_A = 2.5 \times 10^{-9}$ m^2/s.

4. *In vivo* SW-induced cavitation bubble dissolution monitored by B-mode system

4.1. ESWL studies

The *in vitro* studies demonstrated that bubble dissolution processes could be quantitatively detected using B-mode imaging, because the measurements of bubble numbers should be proportional to the area quantification of the hyperechoic regions in the B-mode images. In our previous work, we demonstrated *in vivo* that SW-induced cavitation bubbles indicated by echogenic regions in B-mode images would dissipate gradually after ceasing the SW pulses, which indicated the dissolution of cavitation bubbles.[16] In the present work, these dissolution procedures observed during *in vivo* ESWL studies were further investigated by adopting the decay portions of the temporal evolution curves in Figs. 5(b) and 5c of Ref. [16]. In their experiment, SW-induced cavitation in a pig kidney was mapped by the B-mode imaging system, and the echo areas, which indicated the cavitation activities were processed and plotted versus time, which formed temporal evolution curves of cavitation bubbles. In our work, the time origin ($t = 0$ s) was defined as the point at which the SW pulses stopped in the figures. For the purpose of simulation, all of the decay curves were normalized to their peak values. The simulation results for the cavitation bubble dissolution processes are illustrated in Figs. 3 and 4. In Fig. 3, when the lithotripter was operating at a charging voltage = 24 kV and a PRF = 2 Hz, SW-induced cavitation bubbles dissolved within approximately 15 s. The experimental data can be fitted with the simulated dissolution curve with the parameter set of $R_0 = 35$ μm, the standard deviation of bubbles distribution $SD = 10$ μm, and the diffusion constant $D_A = 5 \times 10^{-7}$ m^2/s. However, close to the 'tail' of the bubble dissolution process, the experimental data do not follow the simulation curve, which continues to trend downward. The experimental and simulated bubble dissolution curves are plotted in Fig. 4, for the cavitation bubbles generated by the SW pulses with a 24-kV charging voltage and a 0.5-Hz PRF. The experimental result was simulated by setting $R_0 = 20$ μm, $SD = 8$ μm, and the $D_A = 2.5 \times 10^{-7}$ m^2/s. Unlike Fig. 3, the experiment dissolution curve in Fig. 4 was fitted very well with the simulation result, even for the times in the range of 10 s–25 s.

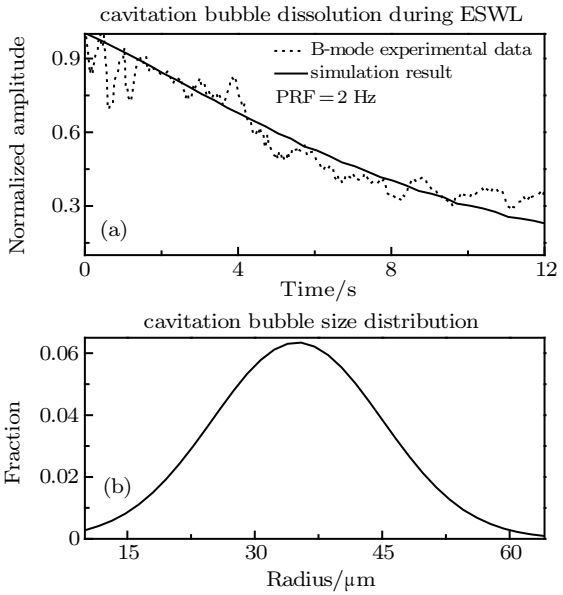


Fig. 3. Experimental data and simulation result for the dissolution of cavitation bubbles generated during an ESWL pig experiment with the lithotripter charging voltage = 24 kV and using a PRF of 2 Hz. (a) The experimental bubble dissolution curve and the simulation results. The experimental data could be best fitted with the selected parameter sets: the mean diameter of bubbles $R_0 = 35$ μm, the standard deviation of bubbles distribution $SD = 10$ μm, and the diffusion constant $D_A = 5 \times 10^{-7}$ m^2/s. (b) The bubble size distribution.

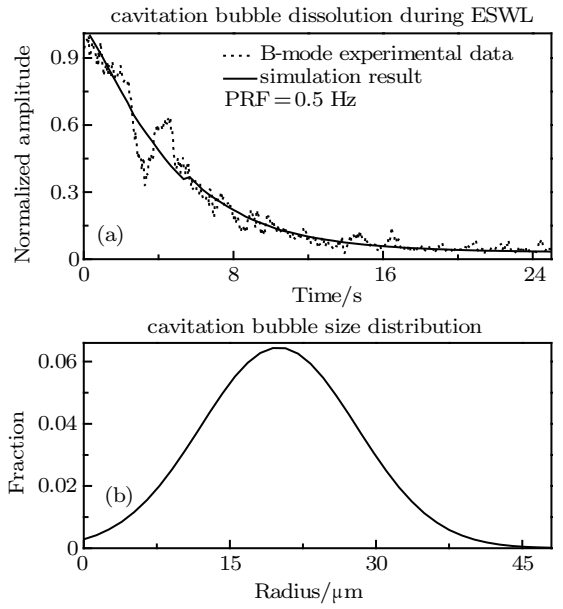


Fig. 4. Experimental data and simulation result for the dissolution of cavitation bubbles generated during an ESWL pig experiment with the lithotripter charging voltage = 24 kV and using a PRF of 0.5 Hz. (a) The experimental bubble dissolution curve and the simulation results. The experimental data could be best fitted with the selected parameter sets: the mean diameter of bubbles $R_0 = 20$ μm, the standard deviation of bubbles distribution $SD = 8$ μm, and the diffusion constant $D_A = 2.5 \times 10^{-7}$ m^2/s. (b) The bubble size distribution.

4.2. ESWT studies

4.2.1. Data acquisition for ESWT

The B-mode images shown in Fig. 5 were taken during the ESWT treatment of plantar fascilitis by using a FDA ap-

proved device (Dornier Epos Ultra, American Kidney Stone Management, Inc. Germany). The Epos machine incorporates an ultrasound imaging system to visualize the plantar fascia and align the shock wave focus. The entire treatment lasted about 20 min, and short-duration ultrasound movies were downloaded to a laptop before, during, and immediately after treatment for off-line image analysis. Figure 5 shows two still frames: one was taken before a procedure started (Fig. 5(a)); another was taken near the end of the procedure (about 20 min later). The circles represent identical ROIs and the cursors represent the focus (Fig. 5(b)). The hyperechoic region observable in Fig. 5(b) is consistent with the appearance of cavitation bubbles. These B-mode movies were recorded to a PC at a frame rate of 30 frames/s, then, post-processed to quantify the area of cavitation bubbles as a function of time, based on the analysis of the characteristics of the hyperechoic regions.

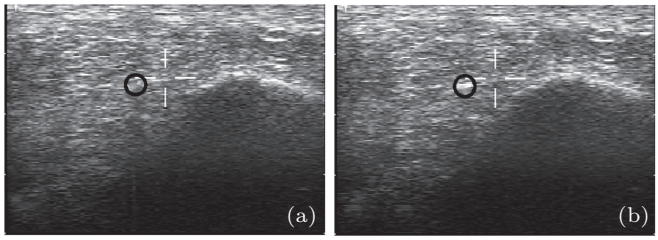


Fig. 5. B-mode images taken in patients during ESWT (plantar fasciitis treatment): (a) before the treatment; (b) near the end of the treatment.

4.2.2. Experimental results

The B-mode movies taken during the ESWT treatments were analyzed using the same method that was applied to the *in vivo* ESWL data. The areas of hyperechoic regions were quantified in terms of pixels, then, were plotted as a function of time in Fig. 6. The figure shows that SW-induced cavitation bubbles grew progressively with delivered SW pulses. Then, the bubble dissolution procedure could be observed as the decay of the hyperechoic region areas.

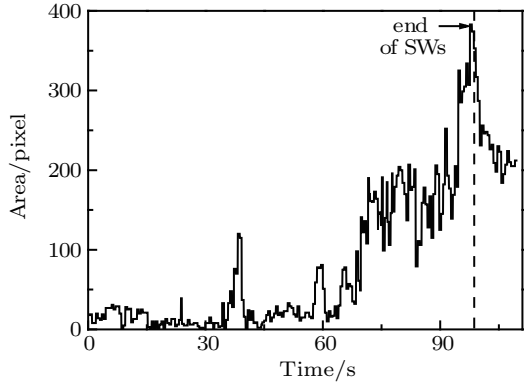


Fig. 6. The temporal evolution of the SW-induced cavitation bubbles during ESWT.

In detail, the dissolution procedure of induced cavitation bubbles during ESWT was investigated after normalizing the decay portion of the temporal evolution curve of the hyperechoic region measurements for the ESWT studies, as described in the ESWL studies. The time origin ($t = 0$ s) was defined as the point at which the SW pulses stopped (viz., marked by the dash line in Fig. 6 that indicates the end of SWs). Figure 7 illustrates the measured bubble dissolution curve and the simulation result for the clinical ESWT study. The figure shows that the simulation result is in reasonable agreement with the experimental data. The best fitting parameters obtained for the ESWT data were: $R_0 = 12.5$ μm, the standard deviation of bubbles distribution $SD = 7$ μm, and the diffusion constant $D_A = 3 \times 10^{-8}$ m^2/s.

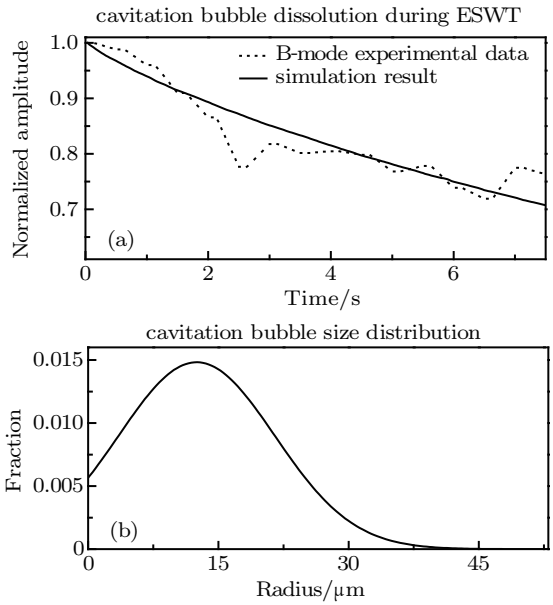


Fig. 7. Experimental data and simulation result for the dissolution of cavitation bubbles generated during clinical ESWT. (a) The experimental bubble dissolution curve and the simulation results. The experimental data could be best fitted with the selected parameter sets: the mean diameter of bubbles $R_0 = 12.5$ μm, the standard deviation of bubbles distribution $SD = 7$ μm, and the diffusion constant $D_A = 3 \times 10^{-8}$ m^2/s. (b) The bubble size distribution.

5. Discussion

It was proved that the single-transducer ACD system was capable of detecting UCA microbubble destruction and the subsequent dissolution process.[24] Here, the dissolution of bi-Spheres bubbles was observed *in vitro* using both ACD and B-mode imaging. The comparison result (Fig. 2) showed that the normalized signals detected by these two systems were in good agreement, which suggested that B-mode imaging was as effective as the single-transducer ACD system. The experimental data were also simulated based on integrated calculation of the scattering cross-section. By setting three fitting parameters (viz., the mean radius of bubbles [R_0], the standard deviation of bubble size distribution [SD], and the gas diffusion constant [D_A]), we assumed that the best simulation result would be obtained when the SDE achieved the minimum value. The results showed that the experimental results for

both two systems could be best simulated with $R_0 = 15$ μm, $SD = 4$ μm, and $D_A = 2.5 \times 10^{-9}$ m^2/s.

Although the results showed that the experimental results could be simulated very well with appropriate fitting parameters, it was of interest to determine if the simulation result was or was not unique, because there were so many parameters involved in the simulation. Figure 8 illustrates the dissolution curve detected by the B-mode system and two simulation curves obtained while using different parameter sets. The SDEs of these two simulation results were both within the range of $(1 + 5\%) \times \mathrm{SDE}_{\min}$. Obviously, similar fitting results could be achieved by introducing different parameter sets. For example, if a larger bubble (e.g., $R_0 = 26$ μm) was assumed and the diffusion constant D_A increased correspondingly (e.g., 10 e^{-9}), the simulated decay curve looked approximately the same as the others. So, how can one determine which simulation result is correct? We should notice that, in Fig. 8, one of the two simulation curves assumed a much bigger bubble and much higher diffusion constant. The air diffusion constant in water under standard conditions (25 °C, 1 atm, 1 atm = 1.01325×10^5 Pa) is 2.4×10^{-9} m^2/s. Therefore, it is applicable to achieve best simulation by adopting the fitting parameters (e.g., $R_0 = 15$ μm, $SD = 4$ μm, and $D_A = 2.5 \times 10^{-9}$ m^2/s) that can generate the minimum SDE. Thus, with the best fitting approach, we could at least get a relatively accurate estimation for the bubble size distribution and the diffusion constant. The parameter SD which presents the deviation of bubble size helps to get the better estimation, although it might not affect the trend of simulation.

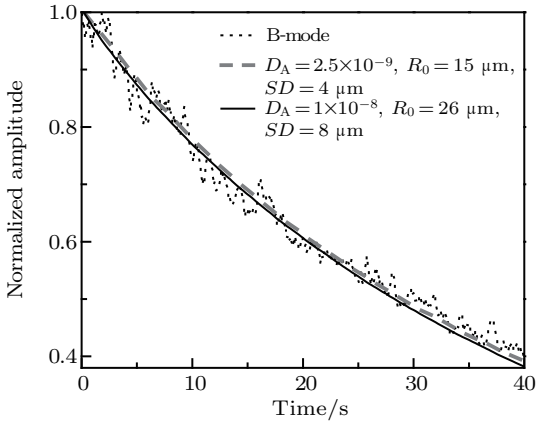


Fig. 8. The dissolution curve measured by B-mode ultrasound. Similar simulation results can be obtained while using different parameter sets.

The above discussion suggests that it is possible to estimate the bubble size distribution and gas diffusion constant by simulating the experimental data properly. Thus, we would like to estimate the size distribution of the cavitation bubbles generated during *in vivo* SW studies by applying this method to the *in vivo* ESWL and ESWT data. Figure 3 shows that, for the ESWL experiment with 2-Hz PRF, the best fitting parameters were $R_0 = 35$ μm, $SD = 10$ μm, and $D_A = 5 \times 10^{-7}$ m^2/s. At 0.5-Hz PRF, the fitting results obtained for the ESWL study (Fig. 4) were $R_0 = 20$ μm, $SD = 8$ μm, and the $D_A = 2.5 \times 10^{-7}$ m^2/s. Figure 7 illustrates that the best fitting parameters for the ESWT data were $R_0 = 12.5$ μm, $SD = 7$ μm, and $D_A = 3 \times 10^{-8}$ m^2/s. Church[28] and Sapozhnilov *et al.*[22] have modeled the dynamic behaviors of the SW-induced cavitation bubbles. Their calculation showed that SW pulses would drive these bubbles into a dramatic growth and collapse followed by a slow dissolution of the bubbles. They also reported that the calculated initial equilibrium radius of the dissolving cavitation bubble in water is ∼ 30 μm, which was at the same order as our estimated bubble equilibrium radius. The maximum diffusion constant for O_2 saturated in whole blood could refer to the order of 10^{-5}. Because the dissolved O_2 concentration in kidney or capillaries could change with conditions, the estimated diffusion constants obtained here are considered to be in a reasonable range, which is greater than 10^{-9} (air diffusion constant in water) and smaller than 10^{-5} (O_2 diffusion constant in whole blood).

The best fitting results for the ESWL pig kidney studies (see Figs. 3 and 4) indicate that, at $t = 0$ s, larger equilibrium diameters of cavitation bubbles were detected by B-mode ultrasound at PRF = 2 Hz. This observation could result from bubble coalescence and is consistent with the results reported in previous literatures.[16,22,29,30] First of all, we have to mention that, due to the slow frame rate of the B-model ultrasound, the R_0 discussed in the current dissolution studies were the equilibrium sizes of residual bubbles after SW pulses. These residual bubbles might be formed by coalescence of small bubbles, which has been observed and described in the optical investigations of Postema *et al.*[29,30] They found that two bubbles will come into contact more quickly if their distance is short. Sapozhnikov *et al.*[22] reported that denser cavitation bubble clouds with larger radii could be observed with the use of higher PRFs. Tu *et al.* also reported similar phenomenon in the ESWL studies based on B-mode imaging quantification analyses.[16] Therefore, it can be postulated that the bubble clouds will be denser when generated at higher PRF, which means more bubbles will be generated with shorter adjacent distance, which would promote bubble coalescence. As a result, the residual bubbles with larger equilibrium radius were generated eventually by the SWs with 2-Hz PRF.

Another interesting point we want to point out here is that, for the experimental data of *in vivo* ESWL at 2-Hz-PRF and ESWT, the tails of the experimental dissolution curves do not follow the simulation results that trend downward continuously. Previous researchers have reported that cavitation bubble nuclei can be stabilized in tissue against dissolution.[31–34] The main possible mechanisms of bubble stabilization have been proposed as: (i) small spherical gas bubbles could be stabilized by a layer of surface-active materials; essentially

shrinking bubbles might be stabilized by a continuous surface formed by molecules;[33] and (ii) cavitation bubble nuclei could be prevented from dissolution if they form inside a crevice.[34] The experimental data tends to approach some stationary minimum values finally, which implied that some forms of "bubble stabilization" might be involved in the dissolution procedure, especially close to the end of the process. However, the experimental data of *in vivo* ESWL at 0.5-Hz-PRF met the simulation result pretty well. As mentioned in the researches of Postema *et al.*,[29,30] sound pressure could drive two bubbles into each other, furthermore, if the distance between two bubbles gets shorter, they may come into contact with each other faster. Meanwhile, larger and more densely populated cavitation bubble clouds were observed in SWL at higher PRF,[22] which in turn had shorter distance between bubbles. By their studies, one could conclude that there were less cavitation events and little residual bubbles at slower PRF. Therefore, the dissolution process at slower PRF (e.g., 0.5 Hz) followed the simulation results better than higher PRF (e.g., 2 Hz).

6. Conclusion

This study investigated dissolution processes of cavitation bubbles generated during *in vivo* SW -induced treatments. Firstly, the feasibility of detecting the bubble dissolution process based on the B-mode imaging technique was confirmed by comparing with the ACD system in the *in vitro* experiments. Secondly, the SW-induced cavitation bubbles dissolution processes were detected by the B-mode imaging system during *in vivo* SW treatments (ESWL and ESWT). Finally, the dissolution processes were simulated to study the characteristics and behaviors of the residual bubbles. The results showed that (I) B-mode imaging technology is an effective tool to monitor the temporal evolution of cavitation bubbles dissolution procedures after the SW pulses ceased, which is important for evaluation and controlling the cavitation activity generated during subsequent SW treatments within a treatment period; (II) the cavitation bubble dissolution procedure detected by B-mode ultrasound can be simulated based on the calculation of the scattering cross-section with employing gas bubble dissolution equations and Gaussian bubble size distribution; (III) the characteristics of the bubbles, such as the bubble size distribution and gas diffusion, can be estimated by simulating the experimental data properly. In summary, this study showed the promising future of estimating the size distribution of SW-induced cavitation bubbles and other involved coefficients, by simulating the bubble dissolution procedures. This work should be helpful for understanding the time-varying SW-induced cavitation activity, which is important for controlling the effects of SW treatments. Furthermore, it may provide a possible method to achieve an optimal SW treatment of minimizing tissue injury without compromising the therapeutic effect by adjusting the dissolving process of residual cavitation bubbles between two sequent SWs.

References

[1] Zderic V, Keshavarzi A, Noble M L, Paun M, Sharar S R, Crum L A and Martin R W 2006 *Ultrasonics* **44** 46
[2] Liu T H, Hao Z Q, Gao X, Liu Z H and Lin J Q 2014 *Chin. Phys. B* **23** 085203
[3] Crum L A 1988 *J. Urol.* **140** 1587
[4] Pitt W G, Husseini G A and Staples B J 2004 *Expert Opin. Drug. Deliv.* **1** 37
[5] Brown M R D, Farquhar-Smith P, Williams J E, ter Haar G and de Souza N M 2015 *Br. J. Anaesth.* **115** 520
[6] Evan A P, Willis L R, McAteer J A, Bailey M R, Connors B A, Shao Y Z, Lingeman J E, Williams J C, Fineberg N S and Crum L A 2002 *J. Urol.* **168** 1556
[7] Zhou Y F, Qin J and Zhong P 2012 *Ultrasound Med. Biol.* **38** 601
[8] Zhang L, Wang X D, Liu X Z and Gong X F 2015 *Chin. Phys. B* **24** 014301
[9] Skolarikos A, Alivizatos G and De La Rosette 2006 *J. Eur. Urol.* **50** 873
[10] Evan A P, Willis L R, Lingeman J E and McAteer J A 1998 *Nephron* **78** 1
[11] Qiao Y Z, Yin H, Li Z P and Wan M X 2013 *Ultrason. Sonochem.* **20** 1376
[12] Delius M 1997 *Ultrasound Med. Biol.* **23** 611
[13] Paterson R F, Lifshitz D A, Lingeman J E, Evan A P, Connors B A, Fineberg N S, Williams J C Jr and McAteer J A 2002 *J. Urol.* **168** 2211
[14] Zhong P and Zhou Y F 2001 *J. Acoust. Soc. Am.* **110** 3283
[15] Zhou Y F and Zhong P 2003 *J. Acoust. Soc. Am.* **113** 586
[16] Tu J, Matula T J, Bailey M R and Crum L A 2007 *Phys. Med. Biol.* **52** 5933
[17] Brennen C E 2002 *J. Fluid Mech.* **472** 153
[18] Pishchalnikov Y A, Williams J C and McAteer J A 2011 *J. Acoust. Soc. Am.* **130** EL87
[19] Pishchalnikov Y A, Sapozhnikov O A, Bailey M R, Pishchalnikova I V, Williams J C and McAteer J A 2005 *Acoust. Res. Lett. Online* **6** 280
[20] Duryea A P, Roberts W W, Cain C A, Tamaddoni H A and Hall T L 2014 *J. Endourol.* **28** 90
[21] Duryea A P, Roberts W W, Cain C A, Tamaddoni H A and Hall T L 2015 *IEEE Trans. Ultrason. Ferroelectr. Freq. Control* **62** 896
[22] Sapozhnikov O A, Khokhlova V A, Bailey M R, Williams J C, McAteer J A, Cleveland R O and Crum L A 2002 *J. Acoust. Soc. Am.* **112** 1183
[23] Epstein P S and Plesset M S 1950 *J. Chem. Phys.* **18** 1505
[24] Chen W S, Matula T J and Crum L A 2002 *Ultrasound Med. Biol.* **28** 793
[25] Bailey M R, Pishchalnikov Y A, Sapozhnikov O A, Cleveland R O, McAteer J A, Miller N A, Pishchalnikova I V, Connors B A, Crum L A and Evan A P 2005 *Ultrasound Med. Biol.* **31** 1245
[26] Church C C 1995 *J. Acoust. Soc. Am.* **97** 1510
[27] Hoff L, Sontum P C and Hovem J M 2000 *J. Acoust. Soc. Am.* **107** 2272
[28] Church C C 1989 *J. Acoust. Soc. Am.* **86** 215
[29] Postema M, Bouakaz A, Chin C T and de Jong N 2003 *IEEE Trans. Ultrason. Ferroelectr. Freq. Control* **50** 523
[30] Postema M, van Wamel A, Lancée C T and de Jong N 2004 *Ultrasound Med. Biol.* **30** 827
[31] Crum L A 1979 *Nature* **278** 148
[32] Crum L A and Mao Y 1996 *J. Acoust. Soc. Am.* **99** 2898
[33] Van Liew H D and Raychaudhuri S 1997 *J. Appl. Physiol.* **82** 2045
[34] Chappell M A and Payne S J 2006 *Resp. Physiol. Neurobi.* **152** 100